DEBRIS ATTITUDE MOTION MEASUREMENTS AND MODELLING

SUMMARY REPORT

ESA/ESOC 4000112447/14/D/SR

Version 1.0

Bern, 09-Sep-2017

Authors	**Responsibility**
J. Silha, R. Kanzler, P. Karrang, A. Breslau, G. Kirchner, M. Steindorfer, D. Cerutti-Maori, J. Rosebrock	J. Silha, T. Schildknecht
Verified	
T. Schildknecht	AIUB study manager
Approved	
T. Schildknecht	AIUB study manager

DOCUMENT CHANGE RECORDS

Version	Date	Changes
Version 0.1	Sep 04 2017	Initial version
Final version	Sep 09 2017	Final version

LIST OF CONTENTS

LIST OF ABBREVIATIONS

AIUB	Astronomical Institute of the University of Bern
ADR	Active Debris Removal
ADU	Analog-to-Digital Unit
CCD	Coupled-Charged Devices
COM	Center of Mass
DIMM	Differential Image Motion Monitor
DLR	Deutschen Zentrums für Luft- und Raumfahrt
ECI	Earth-Centred Inertial
ESA	European Space Agency
FFT	Fast Fourier Transform
FHR	Fraunhofer Institute for High Frequency Physics and Radar Techniques
FoV	Field of View
FPGA	Field Programmable Gate Array
GEO	Geostationary Earth Orbit
GTO	Geostationary Transfer Orbit
ILRS	International Laser Ranging Service
ISAR	Inverse Synthetic Aperture Radar
IQOQI	The Institute for Quantum Optics and Quantum Information
IWF	Space Research Institute of the Austrian Academy of Sciences
LEO	Low Earth Orbit
LOS	Line Of Sight
LVLH	Local Vertical, Local Horizontal
MASTER	Meteoroid and Space Debris Terrestrial Environment Reference
ML	Maximum Likelihood
MOI	Moments Of Inertia
PDM	Phase Dispersion minimization
PROOF	Program for Radar and Observation Forecasting
RAAN	Right Ascension of Ascending Node
RCS	Radar Cross Section
R/B	Rocket Body
SA	Spin Axis
SAR	Synthetic Aperture Radar
sCMOS	Scientific Complementary Metal–Oxide–Semiconductor
SoW	Statement of Work

SLR	Satellite Laser Ranging
SNR	Signal-to-Noise Ratio
TEME	True Equator, Mean Equinox
TIRA	Tracking and Imaging Radar
UTC	Coordinated Universal Time
WGM	Wire-Grid Model
ZIMLAT	Zimmerwald Laser and Astrometric Telescope

1 INTRODUCTION

1.1 Purpose of Document

This is a Summary report of the ESA study "Debris Attitude Motion Measurements and Modeling" (ESA AO/1-7803/14/D/SR) dedicated to the attitude determination of large spacecraft and upper stages. Two major goals have been defined for this project. First, the determination of the attitude motion vector in case of a contingency situation, when a short response time is required between the observations themselves and the attitude determination. The second goal is the long-term prediction (e.g. 10 years) of the spin rate of selected targets for future potential Active Debris Removal (ADR) missions. The study should in particular fuse the results from passive optical, laser ranging and radar observations. We will discuss a highly modular software tool named IOTA (In-Orbit Tumbling Analysis) which was developed during the presented activity. This tool performs short- (days) to long-term (years) propagations of the orbit and the attitude motion of spacecraft in Earth orbit and furthermore its post-processing modules will generate synthetic measurements, i.e. light curves, satellite laser ranging (SLR) residuals and synthetic radar images. We will present results from a collaborative campaign when four priority targets have been selected for collaborative measurements with radar, SLR and light curves in order to test and validate the IOTA tool.

1.2 Documents

1.2.1 Applicable Documents

The following documents contain requirements, which are applicable to this document:

Ref.	Title	Issue
[AD-1]	Debris Attitude Motion Measurements and Modeling, Statements of Work, GSTP-MES-SOW-00115-HSO-GR, Issue 1.0	2014
[AD-2]	Debris Attitude Motion Measurements and Modeling, Technical proposal	2014
[AD-3]	Debris Attitude Motion Measurements and Modeling Description and Schedule of Work dated 8 Oct. 2015, Annex B of the contract between AIUB and Fraunhofer FHR	2015
[AD-4]	Specifications for sensors upgrades, v2.0, Technical note, DD-0003, ESA/ESOC 4000112447/14/D/SR	2016
[AD-5]	Debris Attitude Motion Measurements and Modeling, IOTA Test Report, ESA/ESOC 4000112447/14/D/SR	2017
[AD-6]	Impulse transfer and momentum changes, Technical note 2, v1.0, ESA/ESOC 4000112447/14/D/SR	2015
[AD-7]	Final report, v0.3, ESA/ESOC 4000112447/14/D/SR	2017

Table 1-1: Applicable documents.

1.2.2 Reference Documents

The following documents contain relevant information:

Ref.	Title	Issue
[RD-1]	J. Silha, T. Schildknecht, J.N. Pittet, A. Rachman, M. Hamara, Extensive light curve database of Astronomical Institute of the University of Bern, Proceedings of 7th European Conference on Space Debris, Darmstadt, Germany, 2017.	2017
[RD-2]	Larsson S., *Parameter Estimation in Epoch Folding Analysis*, Astronomy and Astrophysics, 1996, Supplement series 117, 197-201.	1996

Ref.	Title	Issue
[RD-3]	M.A. Earl and G.A. Wade, Observation and Analysis of the Apparent Spin Period Variations of Inactive Box-wing Geosynchronous Resident Space Objects, Proceedings of 65th International Astronautical Congress, Toronto, Canada, 2014, IAC-14-A6.9.1.	2014
[RD-4]	D. Kucharski et al., Attitude and Spin Period of Space Debris Envisat Measured by Satellite Laser Ranging, IEEE Transactions on Geoscience and Remote Sensing, 2014 Dec, v. 52, p. 7651-7657, 10.1109/TGRS.2014.2316138.	2014
[RD-5]	W. H. Press et al., Numerical recipes in C: the art of scientic computing.	1992
[RD-6]	http://ch.mathworks.com/help/signal/ref/periodogram.html	2015
[RD-7]	P. D. Welch, The use of Fast Fourier Transform for the estimation of power spectra: a method based on time averaging over short, modied periodograms," IEEE Transactions on Audio and Electroacoustics, 1967, Volume AU-15, Number 2.	1967
[RD-8]	J. Laer and T. D. Kinman, An RR lyrae star survey with the Lick 20-inch astrograph II. The calculation of RR lyrae periods by electronic computer," American Astronomical Society, 1964, 1965ApJS...11..216L.	1965
[RD-9]	S. Larsson, Parameter estimation in Epoch folding analysis," Astronomy and Astrophysics, 1996, Supplement series 117, 197-201.	1996
[RD-10]	D. A. Leahy, Searches for pulsed emission: improved determination of period and amplitude from Epoch folding for sinusoidal signals," Astronomy and Astrophysics, 1986, 180, 275-277 (1987).	1987
[RD-11]	Kucharki D. et al., Attitude and Spin Period of Space Debris Envisat Measured by Satellite Laser Ranging, IEEE TRANSACTIONS ON GEOSCIENCE AND REMOTE SENSING, 2014, VOL. 52, NO. 12.	2014
[RD-12]	Virgili, B.B., Lemmens, S., Krag, H., Investigation on Envisat attitude motion, e.Deorbit Workshop, 06th of May 2014, Noordwijkerhout, Netherlands, 2014.	2014
[RD-13]	K. Merz, D. Banka, R. Jehn, M. Landgraf, J. Rosebrock (2005). Observations of interplanetary meteoroids with TIRA, *Planetary and Space Science*, **53**, 1121–1134.	2005
[RD-14]	D. Mehrholz. (1996). Ein Verfolgungs- und Abbildungsradarsystemzur Beobachtung von Weltraumobjekten, *Frequenz*, 50:138–146, July 1996. doi:10.1515/FREQ.1996.50.7-8.138.	1996
[RD-15]	Wiedemann, C., et al., The space debris environment model MASTER-2009, 28th International Symposium on Space Technology and Science (ISTS), 5-12 June 2011, Okinawa, paper 2011-r-22, 2011.	2011
[RD-16]	Virgili, B.B., et al., Investigation on Envisat attitude motion, e.Deorbit Workshop, 06th of May 2014, Noordwijkerhout, Netherlands.	2014

Table 1-2: Reference documents.

2 OBSERVATION TECHNIQUES

The population of space debris increased drastically during the last years. Catastrophic collisions involving massive objects produce large number of fragments leading to significant growth of the space debris population. An effective remediation measure to stabilize the population in Low Earth Orbit (LEO) is therefore the removal of large, massive space debris. Secondly, satellite malfunctions might lead to loss of contact with the spacecraft and an accurate attitude determination can help to identify the cause. Such scenarios are referred to as contingency cases.

The attitude states of space objects can be estimated from several types of measurement by using the corresponding processing methods. Some of them can provide direct information about the object spin behavior, like SLR measurements to cooperative targets or Inverse Synthetic Aperture Radar (ISAR) images performed by radar. Direct optical imaging after processing may provide similar results as the ISAR images. Most cost effective for long term monitoring of the objects behavior and its changes are optical telescope measurements, when a light curve of the object is acquired. By applying time series analysis tools one can extract the rotational frequencies from light curves.

All the mentioned measurement techniques will be discussed in more detail in following sections.

2.1 Light curves

The photometric measurement acquisition is the most cost effective observation technique from all here discussed techniques. The output of a photometric data is the brightness variation during the measurement time. i.e. a light curve. Light curves can be acquired for any type of object which is illuminated by the Sun and is reflecting enough light to be visible from the ground instrument. For targets, such as rotating spacecraft, upper stages, and debris pieces, a sequence of photometric measurements is acquired within a short time interval (few minutes) with a short time step (few seconds), depending on the orbit and attitude of the target. Light curves can provide directly the apparent (synodic) rotation (spin). Apparent period is a direct function of the object's own rotation period also referred to as the sidereal period. Light curves are strongly related to the rotation of the observed object. To be able to analyze light curves obtained by optical measurements, i.e. determining the rotation period and the rotation axis direction, several methods can be applied [RD-1].

2.1.1 CCD/CMOS light curves

Photometric data acquisition can be performed by using optical telescope along with the CCD (Charge-Coupled Device) or CMOS (Complementary Metal-Oxide-Semiconductor) sensors. Once these types of sensors are used the photometric reduction can be performed and the ADU (Analog Digital Unit) units can be recalculated to the astronomical magnitude units. An example of a light curve for GLONASS satellite 2001-053C acquired by AIUB's ZIMLAT system (see section 4.1.1) is plotted in Figure 2-1.

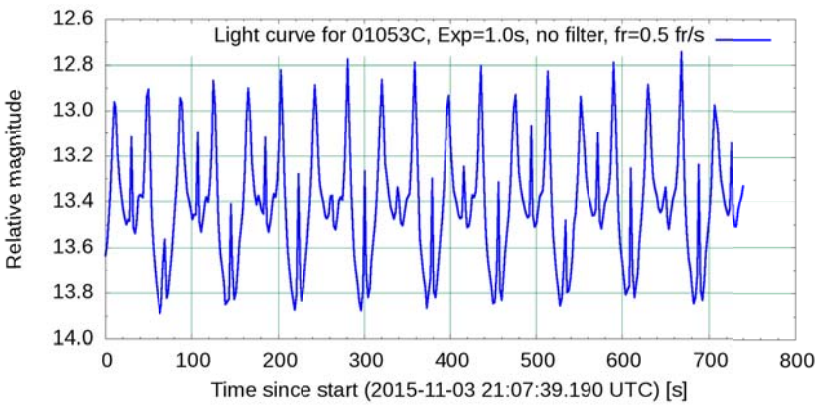

Figure 2-1: Light curve for GLONASS satellite 2001-053C acquired by AIUB's ZIMLAT system.

2.1.2 Light curves processing

For the processing of light curves acquired by CCD or CMOS cameras refer to [AD-4].

2.1.3 Single-photon light curves

The light curve measurement system setup at the Graz SLR station can be explained according to the schematics (Figure 2-2). Light gathered by the receiving optics of the telescope is filtered in advance and only a wavelength range between 780-1000 nm is passed on to the light curve detection system. The laser wavelengths 532 nm and 1064 nm are simultaneously used for satellite laser ranging (SLR) measurements. This points out a very important feature: Light curves are measured simultaneously and independent from SLR.

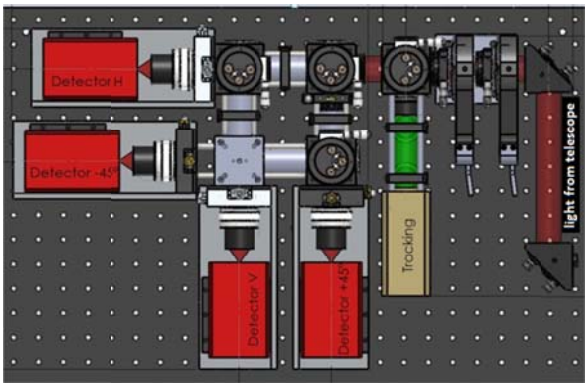

Figure 2-2: Schematics of the light curve measurement system at SLR station Graz using siingle photon avalanche diodes.

The signal is measured by SPAD detector and then evaluated and run in two different modes:

a) The total number of photons received is counted per bin (with arbitrary sizes; for most of the experiments 10 ms bin size turned out to be a reasonable value)

b) The epoch times of all photons are recorded up to a resolution of 25 µs (limited by the response time of the FPGA)

The data is then transferred to a brick-PC and stored on disk. Figure 2-3 shows a typical example of a light curve of Topex (NORAD ID: 22076) recorded on day 175 of the year 2015. The y-axis displays the number of photons detected within an interval of 10 ms, the x-axis is the time [s] since the beginning of the light curve measurement. A closer look at the signal (Figure 2-4) reveals details of the reflecting surfaces of the satellite and clearly shows a four-way symmetry.

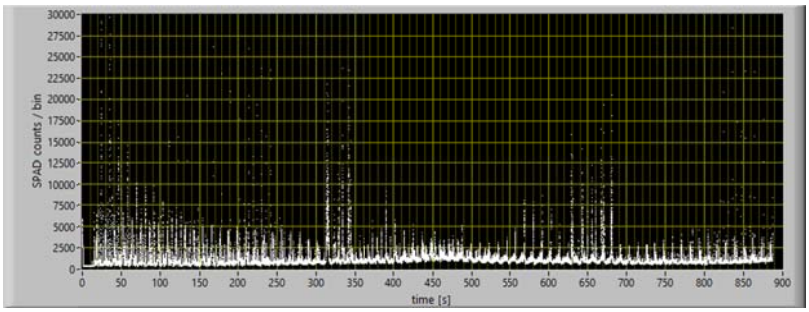

Figure 2-3: Typical example of a light curve of Topex recorded on day 175/2015 covering approx. 900 s.

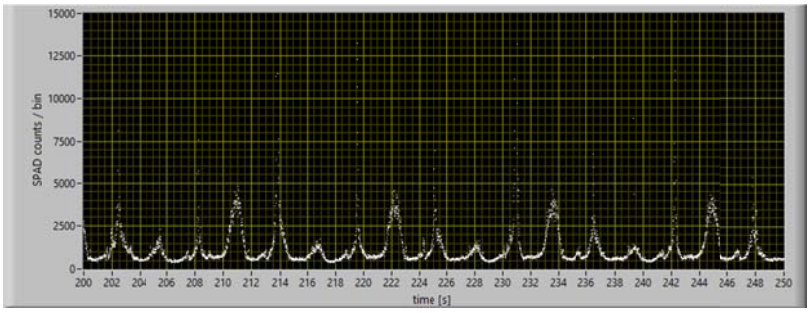

Figure 2-4: Close-up of the light curve of Topex recorded on day 175/2015 covering 50 s.

Data analysis theory

For data analysis theory refer to [AD-4].

Routine light curve measurements

Graz routinely measures light curves to selected spinning uncooperative targets and evaluates their spin behavior according to the previously mentioned methods. A typical normalized light curve of the Compass G2 satellite (NORAD ID: 34779) shows four distinct peaks (Figure 2-5) corresponding to four sides of the satellite according to its box-wing shape. Its rotational period is determined to be T = 7.14 s.

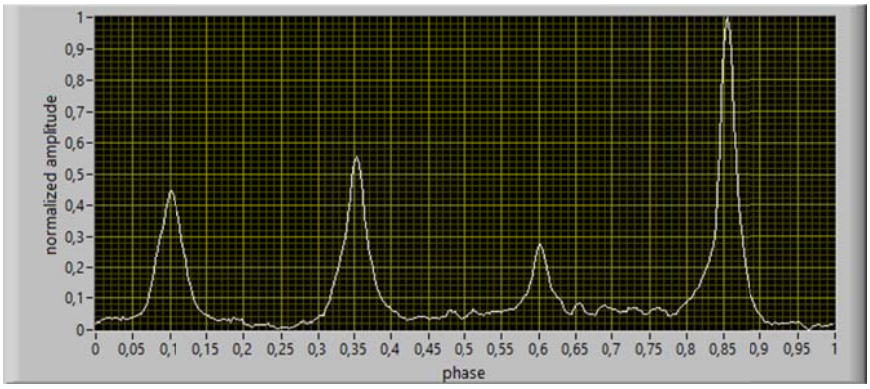

Figure 2-5: Mean light curve of the Compass G2 satellite for the interval between 200 and 300 s. The phase on the x-axis ranging from 0 to 1 corresponds to the spin period of T=7.14 s which was determined by using the autocorrelation function and phase dispersion minimization algorithm.

Using light curve- and laser-based spin period measurements the rotation period of more than 40 defunct Glonass satellites were measured revealing differences between approx. 8 and 400 s.

Furthermore, seasonal variations were discovered e.g. Adeos-2 (NORAD ID: 27597) as shown in Figure 2-6.

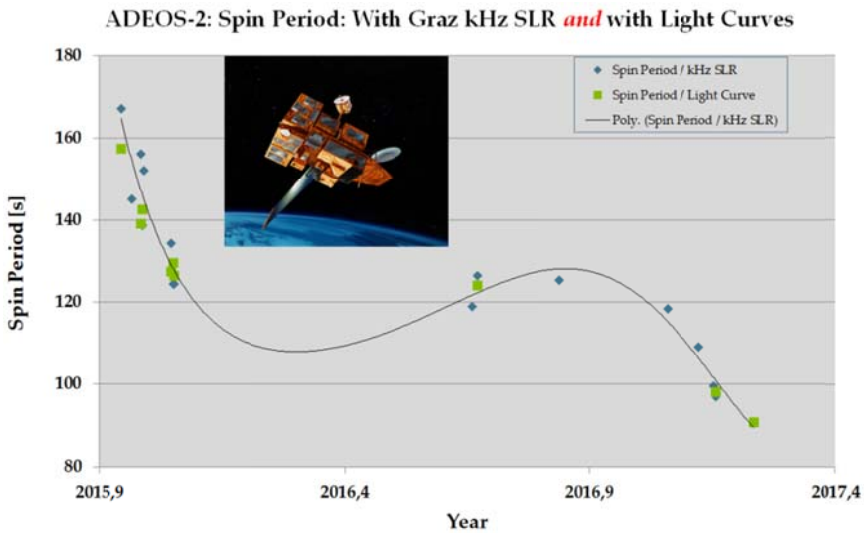

Figure 2-6: Spin variations of Adeos-2 (NORAD ID: 27597) showing seasonal variations.

2.2 Radar measurements

2.2.1 Inverse synthetic radar image

Advantages of radar systems compared to other measurements systems like optical systems are their ability to observe space objects at any time a day independently from the weather conditions.

Inverse synthetic aperture radars (ISAR) exploit the rotational motion between radar and object in order to image the object in 2D. The radar transmits regularly waveforms that are backscattered by the object and received by the radar. From the delay between transmit and receive, the ranges between the radar and the different point scatterers, which are distributed over the object, can be measured. Over time, the object rotation causes small variations of these distances. This induces phase differences between radar pulses that are proportional to cross-range (i. e. direction perpendicular to range). Cross-range positions can therefore be separated by spectral analysis of consecutive pulses.

Challenge of ISAR imaging is the estimation of the unknown object motion from the radar data. Indeed, the kinematics of the object is required in order to form a focused image of the moving object. The motion of the object can be decomposed into a translational motion of a reference point of the object, which has to be compensated, and a rotational motion around an axis through this reference point, which leads to ISAR imaging.

The object is imaged in the so called image plane. The first direction (range) is in the line-of-sight (LOS) direction from the radar to the object. The second direction (cross-range) is orthogonal to the effective rotation vector, which is the component of the rotation vector of the object (w.r.t. a coordinate system aligned with the LOS) orthogonal to the LOS vector. The norm of the effective rotation vector scales the ISAR images in cross-range. The image plane is, hence, the range / cross range plane that is perpendicular to the effective rotation vector and contains the LOS vector. The scatterers of the object are projected to this image plane.

Unfortunately, the image plane and the cross-range scaling of an ISAR image are changing with time and are usually unknown. They depend on the satellite's rotational motion, the satellite's orbit, the radar location and Earth rotation. All, except for the first parameter, are usually known in advance. Therefore, correct cross-range scaling can only be obtained if the rotational motion of the object, i.e. the sequence of its attitudes over time, is known or has been estimated.

2.3 SLR measurements

2.3.1 SLR residual signal, IWF

Graz routinely tracks several defunct satellites equipped with retroreflectors by SLR such as Envisat, Topex, Adeos-2 or various Glonass satellites.

Envisat (NORAD ID: 27386) shows an oscillation of the Observed-Minus-Calculated (O-C) SLR residuals due to the consecutive visibility of its different retroreflectors within the rotation of the satellite within one pass (Figure 2-7). The satellite has 8 retroreflectors equipped on one pyramid and hence the rotation period can be calculated from analyzing the distance between the peaks within the residuals. After the end of the mission in April 2012 from the laser tracking results of over 4 years a trend was derived regarding the spin behavior of the satellite. Soon afterwards within 2 months Envisat started spinning leading to a maximal spin rate of 0.547 rotations per minute (rpm) or T = 110 s. This spin-up period was followed by an exponential loss of rotational energy to approx. 0.3 rps / T = 200 s at the beginning of 2016 (Figure 2-8).

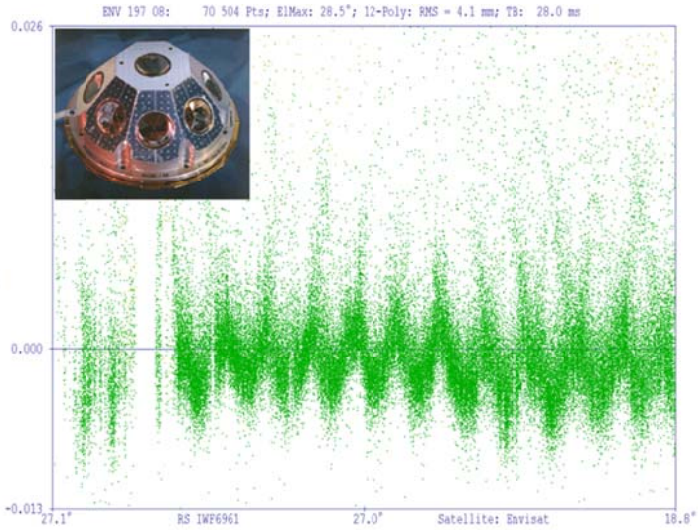

Figure 2-7: Typical SLR O-C residuals of Envisat showing an oscillation due to the 8 retroreflectors on the pyramid shown in the insert.

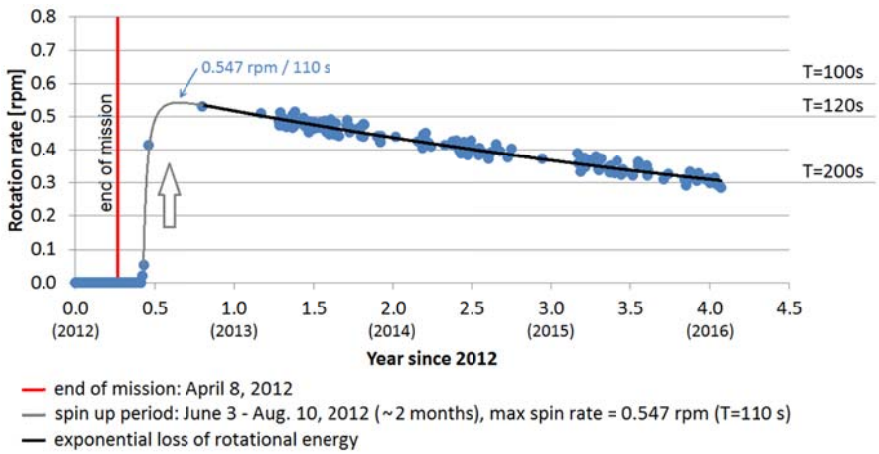

Figure 2-8: Spin-up period of Envisat after the end of the mission in 2012 followed by a continuous decrease of spin rate in the following years.

For ERS-1 SLR data (32 passes) revealed an exponential increase in spin period from approx. 2 min to 6 min within three years from 2013 (Figure 2-9). According to this trend the spin period will become equal to the orbital period in 2021.

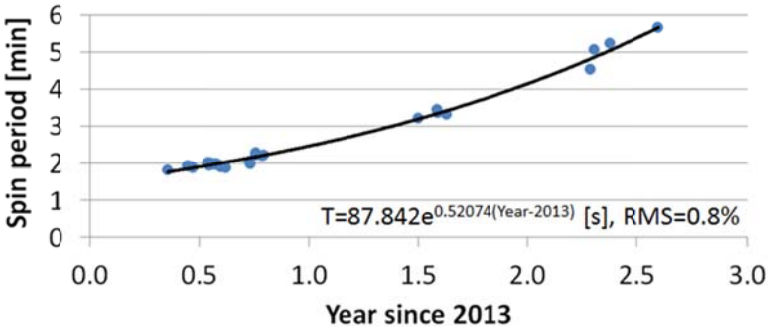

Figure 2-9: Exponential increase of spin period of ERS-1 from the beginning of 2013.

2.3.2 SLR to non-cooperative targets, IWF

The re-entry target rocket body Long March 3B (Norad ID: 38253) having a highly eccentric orbit with an apogee of 1700 km and a perigee of only 147 km (July, 2017) was chosen to show the advantages of performing light curve and space debris laser ranging measurements simultaneously. The rocket body cylinder has a length of 12 m and diameter of 3 m and is not equipped with retroreflectors and is expected to re-enter in August 2017.

SLR data shows clearly an oscillation of 120 s with a maximum amplitude of ± 6 meters (Figure 2-10). The amplitude is increasing throughout the pass.

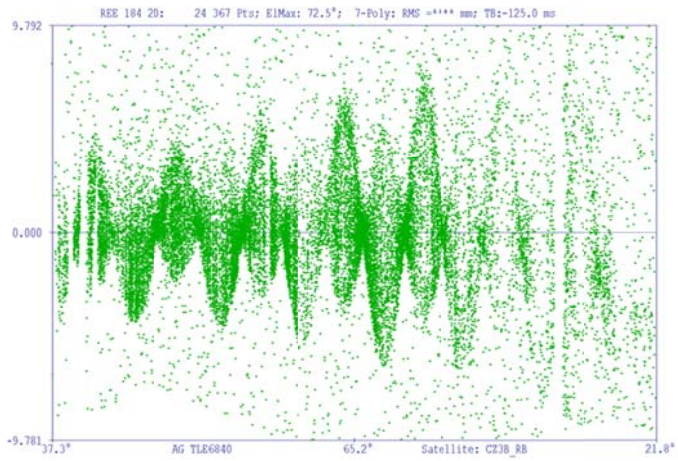

Figure 2-10: SLR range residuals [m] of the Long March 3B rocket body showing a rotation period of approx. 120 s.

Simultaneous plotting of light curve data (white) and SLR range residuals (green) reveals that maximal SLR residuals offsets correspond to minimal light curve photon counts (Figure 2-11, Figure 2-12). This allows the following interpretation: At maximal SLR residuals the cylinder axis has to be close to the line of sight of the observer to yield offset with of amplitudes of ± 6 meters. Vice versa, minimal SLR residuals indicate that the axis of the cylinder is close to a plane normal to the line of sight of the observer. Hence the cylindrical surface contributes to the light curve signal leading to a light curve maximum.

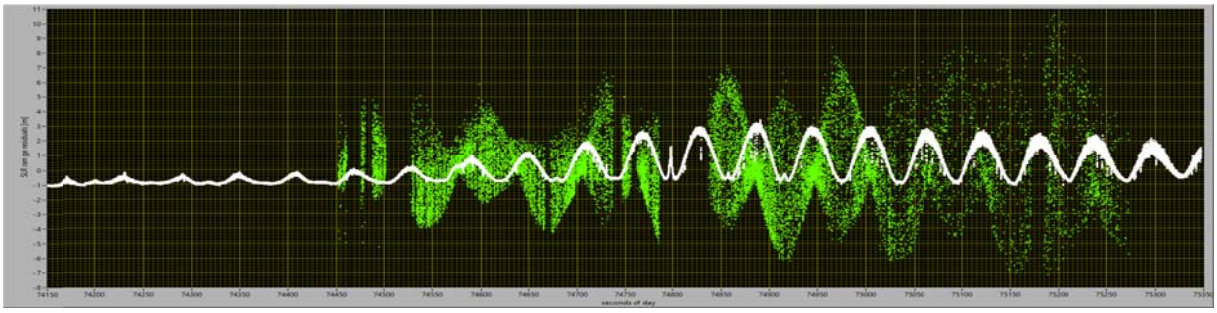

Figure 2-11: Simultaneous display of light curve (white) and SLR O-C residuals (green) over time (seconds of day). The y-axis displays range residuals [m], the light curves are scaled accordingly to fit within the range of the residuals.

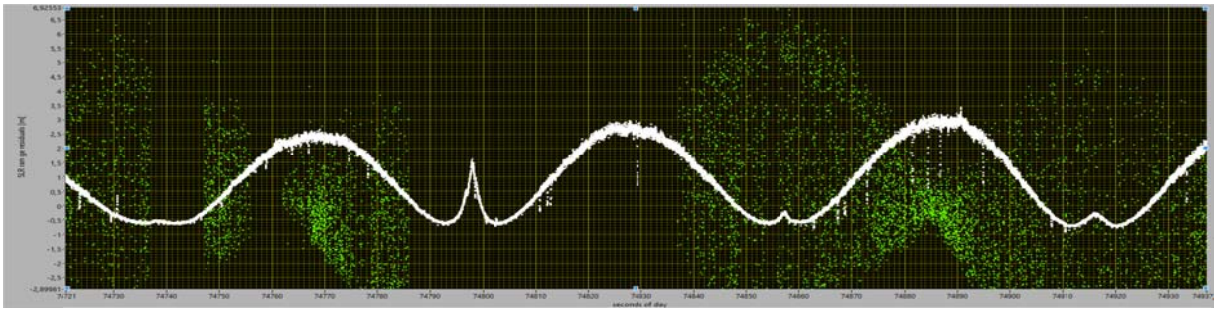

Figure 2-12: Close-up of the simultaneous display of light curve (white) and SLR O-C residuals (green) over time (seconds of day), covering an interval of approx. 200 s. The y-axis displays range residuals [m], the light curves are scaled accordingly to fit within the range of the residuals.

2.3.3 SLR residual signal, AIUB

In following section is discussed the AIUB's method for the attitude determination from satellite laser ranging (SLR) measurements to the defunct satellite ENVISAT (02009A). Method of synthetic ranges and parameter estimation is applied.

2.3.3.1 Parameters definition

Several different parameters are determined during the parameter estimation process. For ENVISAT it is known from different studies [RD-11] that its spin axis is quite stable and almost perpendicular to the orbital plane. Following parameters have been chosen for the investigation:

Observation/measurement/reference time [s] – is the reference epoch, for this epoch determined will be all the parameters

Angles γ [rad] and γ_{phase} [rad] – angles [rad], these are spherical coordinates, elevation and azimuth, defined in the orbital reference frame.

Angles β [rad] and β_{phase} [rad] – angles [rad], these are angles defined in the body fixed coordinate system

Inertial period [s] – rotation period in inertial system

Period phase [rad] – complementary angle defining the current satellite alignment for given measurement time

For presented angles are giving further description below.

Angles γ [rad] and γ_{phase} [rad] – By γ we define an angle between vector perpendicular to the orbital plane $\vec{W} = \vec{r}_{sat}$ x $\vec{v}_{sat}$ and rotation vector $\vec{\omega}$. Angle γ_{phase} starts at direction toward the projection of North to the orbital plane (plane perpendicular to $\vec{W}$) increasing in counter-clockwise direction by using right-hand rule around $\vec{W}$. Angle γ can be within interval $(0; \pi)$ and γ_{phase} can be within interval $(0; 2 * \pi)$.

Angles β [rad] and β_{phase} [rad] – By β we define an angle between rotation vector $\vec{\omega}$ and RRA position vector $\vec{r}_{RRA}$ in the body fixed reference frame. Angle β_{phase} defines the pointing direction of the solid body around $\vec{r}_{RRA}$. For better description we use the ENVISAT's body-fixed reference frame discussed in [RD-11]. In this frame the axis x_{ESA} is passing trough the CoM and it's pointing toward the solar panel, the axis z_{ESA}, which is aligned with the RRA axis of symmetry, is pointing in the opposite direction than the RRA and the axis y_{ESA} is perpendicular to both axes completing the full right-handed coordinate system. If we define a plane perpendicular to $\vec{r}_{RRA}$, the β_{phase} angle is measured from the projection of the x_{ESA} axis into this plane in the counter-clockwise direction toward the y_{ESA}. Angle β can be within interval $(0; \pi)$ and β_{phase} can be within interval $(0; 2 * \pi)$.

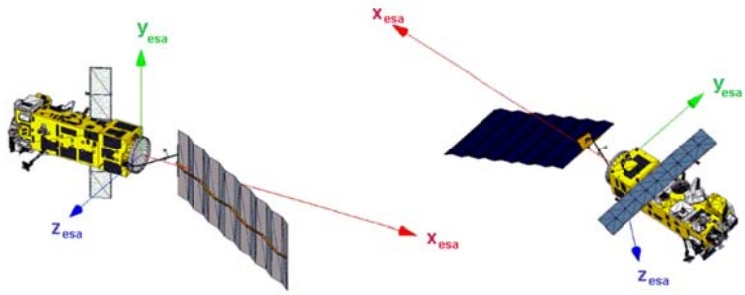

Figure 2-13: ENVISAT's body-fixed reference frame as defined in the [RD-12]. Taken from [RD-12] and modified.

2.3.3.2 Parameters estimation

As an output of the SLR measurements for tumbling objects is the modulation on the range between the laser and the object's RRA. This signal has a specific shape and phase which can be by using a reasonable assumption describe by small number of parameters. In our case these parameters are γ, γ_{phase}, β, inertial period and period phase. In Figure 2-14 is shown an influence of different parameters on the shape of the SLR residuals signal obtained for ENVISAT. Additionally, there is also shown the so-called along-track parameter which is used for the refinement of detrending of the signal during the parameters estimation.

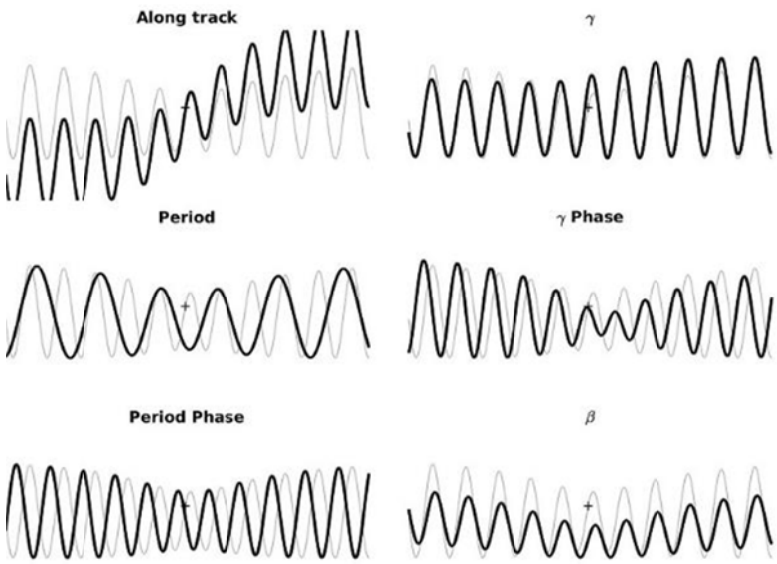

Figure 2-14: Influence of a given parameter on the shape of the measured SLR residuals for ENVISAT.

The goal of the parameter estimation step is to determine mentioned sets of parameters in order to find the best fit between real residuals and the synthetically generated residuals obtained by using given parameters. In our case we performed iterative procedure where for every step we manually adjust given five parameters, we generated synthetic residuals and we compared them to the real residuals and we determine the standard deviation between these two data sets. Once we reached a moment when the standard deviation only changed slightly, e.g. fraction of millimeter, we stopped the procedure and we extracted the determined parameters. An example is plotted in Figure 2-15 for ENVISAT's pass obtained by ZIMLAT at 8th of September 2015. For given pass and

reference epoch we determined the inertial period to be 187.3 s, angle $\gamma = 152° \pm 0.85°$ and angle $\beta = 59.3° \pm 0.73°$.

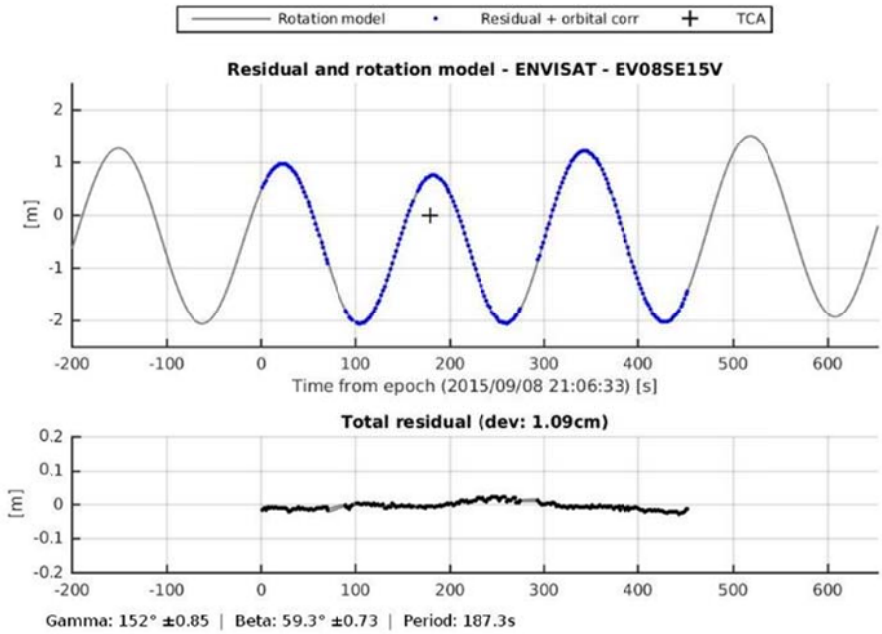

Figure 2-15: Comparison between real residuals and synthetic residuals constructed by using the parameters determined during parameter estimation procedure. Plotted is Zimmerwald ENVISAT pass measured at 8th of September 2015.

To have the attitude model complete, one has to determine the angle β_{phase}. This can be done by using the estimated parameters γ, γ_{phase}, β, inertial period and period phase and by using the information that RRA was visible the whole pass. Once we simulate different β_{phase} angles, from interval $(0; 2 * \pi)$ we found out, that only for an interval $(1.1 * \pi; 1.7 * \pi)$ (interval from 200° to 300°) the RRA would be visible the whole time from Zimmerwald site for given measured fraction of the pass. It seems that the experimental visibility of RRA is in total agreement with the simulated one. By investigating more passes from time interval 2013 to 2015 we found out that this interval was stable during the time. Due to the symmetry of the visibility window we expect for β to be between 200° to 300°, hence $\beta \sim 250°$.

The presented approach for attitude determination from SLR ranges is not directly applicable to every cooperative target and needs to be adopted accordingly, namely the defined model and its parameters must be adopted to the object's RRA type ("point" like RRA like for ENVISAT versus "ring" like RRA for TOPEX/Poseidon), its orbit and its attitude (preliminary assumption). For ENVISAT it was convenient to choose the angles γ and γ_{phase} to be fixed on the orbital plane to minimize the effect of RAAN drift, which is typical for Sun synchronous orbits (SSO). We also knew from other studies that β and rotation vector $\vec{\omega}$ angle are quite stable over time. This might not be case for other targets and for each target an individual interpretation should be chosen.

3 ATTITUDE MOTION MODELING

3.1 In-orbit tumbling analysis tool ıOTA

ıOTA is a prototype simulation software to perform short- (days), medium- (months) and long-term (years) propagations of the orbit and attitude motion (six degrees-of-freedom) of spacecraft in Earth orbit, taking into account all relevant acting forces and torques. It is able to generate synthetic measurement data (light curves, SLR ranges, visual images, simplified radar images and radar cross-section) based on the simulation results in order to enable a direct comparison with real measurement data.

ıOTA is able to run on PCs which meet the following hardware requirements:

- Dual Core Processor with 2.66 GHz
- 4GB of RAM

The supported operating systems are Windows 7 (64-bit) and Suse Linux Enterprise 11 (SP3).

3.1.1 Modular architecture design

The process hierarchy of ıOTA is shown in Figure 3-1. ıOTA is highly modular with a flat hierarchy structure and the calling of the particular software modules is performed by the ıOTA host process, except for the post processing, which is called from the propagator. Figure 3-2 displays the decomposition of the software, including the software modules, the data flow from the model and input data (blue) to the particular modules, as well as the data flow from the simulation (yellow) and propagation (red) modules to the particular destination. The post-processing branch (green) provides the final processing and visualization of the simulation results.

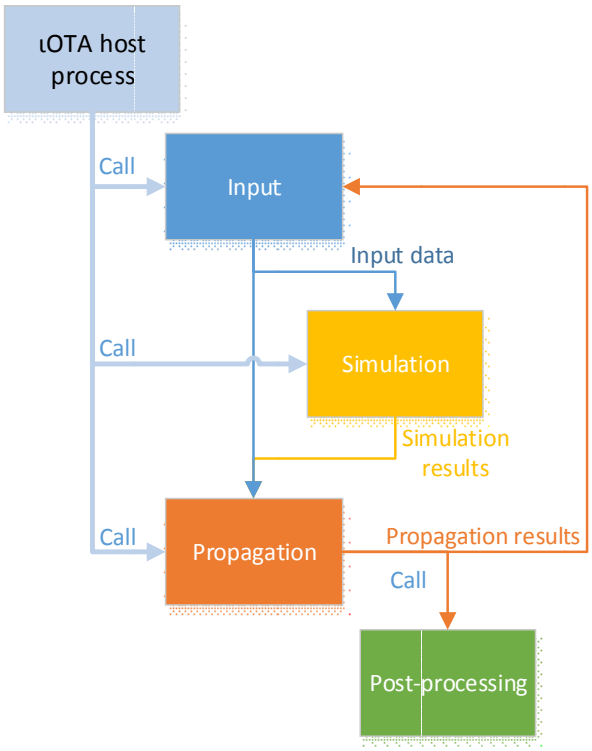

Figure 3-1: ıOTA process hierarchy and functional architecture

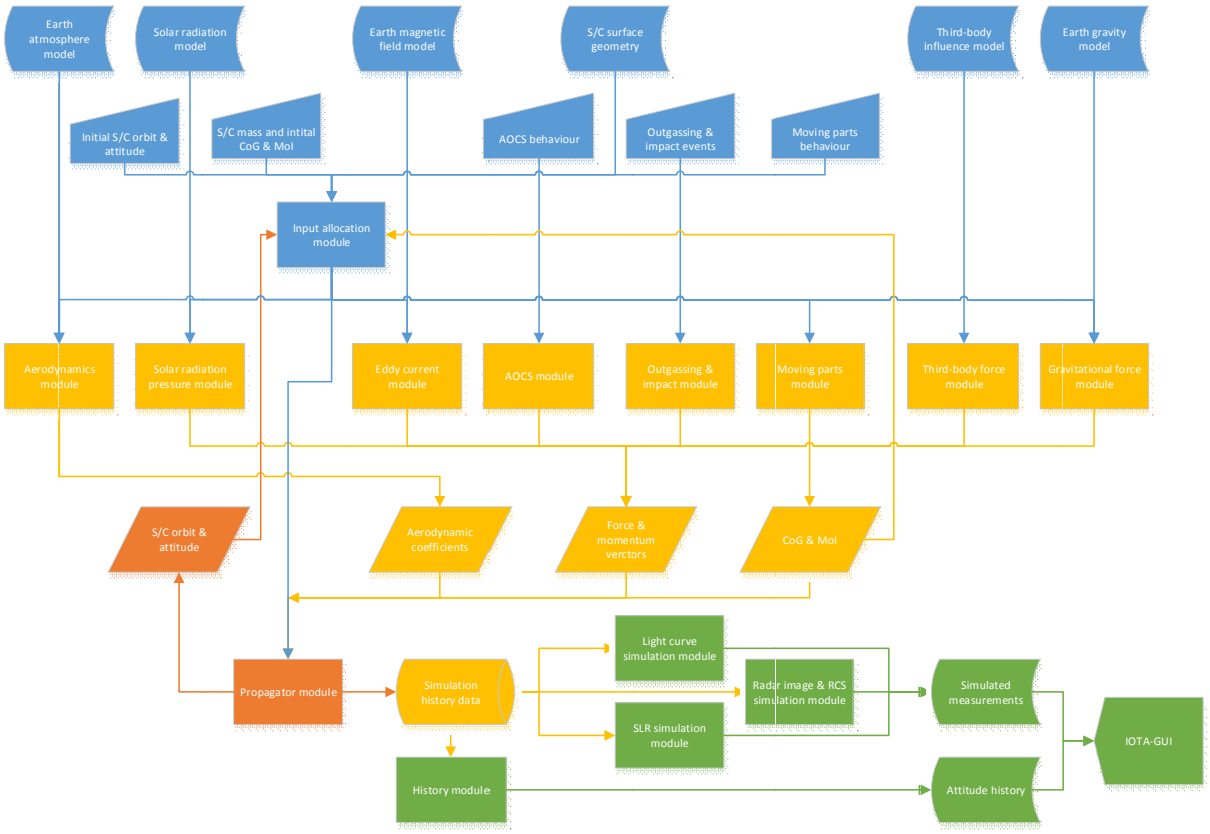

Figure 3-2: IOTA decomposition and interface diagram

The software comprises the following modules

Input modules:

- **Input** – Input allocation module

Simulation modules:

- **3rd-B** – Third-body force module
- **Aero** – Aerodynamics module
- **AOCS** – Attitude and Orbit Control system
- **Eddy** – Eddy current module
- **Grav** – Gravitational module
- **MoveP** – Moving parts module
- **OutIm** – Outgassing and impact module
- **Prop** – Propagator module
- **SolRad** – Solar radiation pressure module

Post-processing modules:

- **History** – History module
- **SimLC** – Simulated measurements module: light curves
- **SimRad** – Simulated measurements module: radar image and RCS
- **SimSLR** – Simulated measurements module: satellite laser ranging

Visualization modules:

- **IOTA-GUI** – IOTA Graphical User Interface

3.1.2 Simulation input and modelling

Apart from the specific configuration of tOTA simulations, which is done via configuration (`.ini`) files, the surface geometry model of the to be simulated spacecraft is needed in either +.obj or +.gpf format, based on triangular panels with panel normal pointing outwards. Events (outgassing, impact, or AOCS) or Tanks (for the simulation of tank sloshing) are specified in lists (`.lst`). All settings files are self-explanatory, in general. The configuration files in the test cases included in the release package, provide pre-configured example settings.

The initial orbit state can be specified either using Kepler orbital elements or an inertial state vector. The initial attitude state is specified using roll, pitch and yaw angles and the corresponding roll, pitch and yaw rates, either relative to the inertial frame or relative to the orbital frame (LVLH).

3.1.3 Simulation output

The simulation history data is stored in the `HISTORY/` subfolder. The simulated measurements are stored in the `OUTPUT/` subfolder. The history and output data is stored in ASCII format. The tOTA-GUI can be used to view the history data and synthetic measurements. For more information about simulation output refer to [AD-7].

3.2 Software validation and testing

In this section we will present long-term prediction for ENVISAT. For more about tOTA software validation refer to [AD-5].

3.2.1.1 ENVISAT

We performed a long-term attitude motion prediction of ENVISAT to validate the tOTA prediction modules. We were interested in monitoring the inertial angular velocity evolution over time. As inputs we had following parameters:

- Initial epoch: 2013-07-13 21:43:12.0
- Initial attitude state: determined from SLR by AIUB
  - Euler angles (roll, pitch, yaw): 0 deg, 0 deg, -78.499deg
- Initial attitude motion state determined from SLR by AIUB
  - Rotation vector (ω_x, ω_y, ω_z): 0 deg/s, 0 deg/s, -2.735 deg/s
- Initial orbit state: generated by using TLE and SGP4 model
- Model: ENVISAT 3D model based on refined SCARAB model
- Simulation time: approx. 400 days

Due to the high processing time consumption we included to the simulation following forces only:

- Gravitational force and torque for the orbit and attitude motion prediction
- 3rd body perturbation for the orbit prediction
- Eddy currents for the attitude motion prediction

Solar radiation pressure and atmospheric drag have been excluded to decrease the processing time. The obtained results have been compared qualitatively, see Figure 3-3, with the values determined by AIUB from SLR residuals measurements acquired to ENVISAT by ZIMLAT telescope in years 2013-2014. Real measurement values are marked by black points in Figure 3-3. Several different combinations of forces acting on the satellite are taken into account. The orange line represents a case when only the gravitational force is included. This force has no influence on the attitude change over time, as expected. The same goes for the 3rd body perturbation marked as green. Once we include eddy currents torques, blue and magenta, the angular velocity decreases over time the similar way as it is for the real measurements (black points).

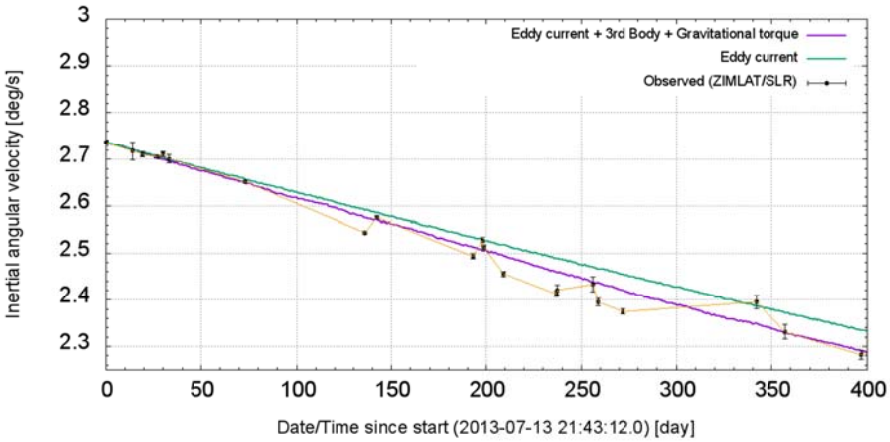

Figure 3-3: Inertial angular velocity of ENVISAT satellite determined by AIUB from the SLR residuals acquired by ZIMLAT system during years 2013 – 2014 (black points) and predicted angular velocity by assuming different acting torques/forces.

4 COLLABORATIVE MEASUREMENTS

4.1 Sensors

Following sections are discussing sensors which were used during the duration of the activity and during the collaborative measurements.

4.1.1 ZIMLAT telescope

One of the main instruments at AIUB's Swiss Optical Ground Station and Geodynamics Observatory Zimmerwald, Switzerland (hereafter called Zimmerwald observatory) (observatory code 026, SLR station code ZIML) is the 1-meter Zimmerwald Laser and Astrometry Telescope (ZIMLAT). ZIMLAT is used either for SLR to cooperative targets, targets equipped with SLR retroreflectors, or for passive optical observations (astrometric positions and magnitudes) of artificial and natural objects in near-Earth space. During daytime the system operates in SLR mode only. During night time the available observation time is shared between SLR and optical observations [RD-1] based on target priorities. The switching between the modes is done under computer control and needs less than half a minute. Telescope is equipped with standard CDD camera FLI SI1100 and with Andor Neo scientific CMOS camera with frame-rates up to the 50 frames/s. The ZIMLAT telescope is shown in Figure 4-1.

Figure 4-1: ZIMLAT telescope during the day when only SLR observations are used (left panel) and a closer look at ZIMLAT telescope during the night when CCD, sCMOS or simultaneous SLR and CMOS observations are used (right panel).

4.1.2 TIRA radar

The space observation radar TIRA (Tracking and Imaging Radar) located in Germany is the largest experimental system which is unique in Europe. It is operated by the Fraunhofer Institute for High Frequency Physics and Radar Techniques FHR. The system primarily serves as the central experimental facility for the development and investigation of radar techniques for the detection and reconnaissance of objects in space. TIRA also provides valuable support for space missions: space agencies from all over the world use the special capabilities of the FHR scientists and their system. As the name implies, the TIRA system comprises a tracking radar and an imaging radar. The narrowband, fully coherent, high power tracking radar has a transmission frequency in L-band (1,333 GHz) and the wideband imaging radar has a transmission frequency in Ku-band (16.7 GHz) and is currently equipped with a high target resolution. TIRA radar is shown in Fig. 4-1.

Figure 4-2: FHR's TIRA system. Photo credit: Fraunhofer FHR

4.1.3 Graz SLR station

Graz SLR station belongs to The Space Research Institute (Institut für Weltraumforschung, IWF) in Graz (Austria). Satellite Laser Ranging (SLR) is a method to measure distances to satellites using very short laser pulses. At the Graz SLR station, a very short laser pulse (10 ps) is generated, transmitted to the satellite, and reflected back to the station, where it is detected. A high precision event timer - using time and standard frequency derived from a special dedicated GPS receiver - measures the time of flight of the laser pulse with an accuracy of about 3 ps. Using the known velocity of light, one can thus determine the distance to the satellites - from a few hundred kilometres up to more than 40,000 km - with an accuracy of a few millimetres.

Figure 4-3: The the 5 m diameter dome of the SLR Graz station including a 0.5 m telescope

The kHz SLR system in Graz delivers data with very high accuracy, and allows – for satellites equipped with retro-reflectors - determination of additional parameters, like spin duration, spin axis orientation, and spin direction.

In order to test laser ranging possibilities to space debris objects, the Satellite Laser Ranging (SLR) Station Graz installed in 2013 by frequency doubled Nd:YAG pulse laser with 100 Hz repetition rate, a pulse width of 3 ns, and a single pulse energy of 200 mJ at 532 nm, also on loan from DLR Stuttgart. IWF developed and built low-noise single-photon detection units to enable laser ranging to targets with inaccurate orbit predictions, and adapted our standard SLR software to include several hundred space debris targets. With this configuration, we successfully tracked - within early-evening sessions of each about 1.5 hours – more than 200 passes of about 60 different space debris targets, in distances between 600 km and up to more than 3000 km, with radar cross sections from > 15 m^2 down to < 0.3 m^2, and measured their distances with an average precision of about 0.7 m RMS.

4.2 Target list

4.2.1 ENVISAT

We defined five priority targets to be observed during simultaneous observations. Because of the high interest, ENVISAT (2001-002A), an ESA satellite which is non-active since 2012, has been selected as priority target. On 8th of April 2012 the Agency lost contact with the satellite. Currently, ENVISAT is one of the largest and heaviest objects in Low Earth Orbit (LEO) region, which is the region with the highest density of man-made objects in space, and poses a big treat to operational spacecraft in case of a collision or break-up event. ENVISAT is orbiting at a mean altitude of 766 km. It is equipped with a RRA which makes is observable by any SLR system, if the RRA is visible from the station. The 3D model of ENVISAT satellite used in the ıOTA tool is plotted in Figure 4-4.

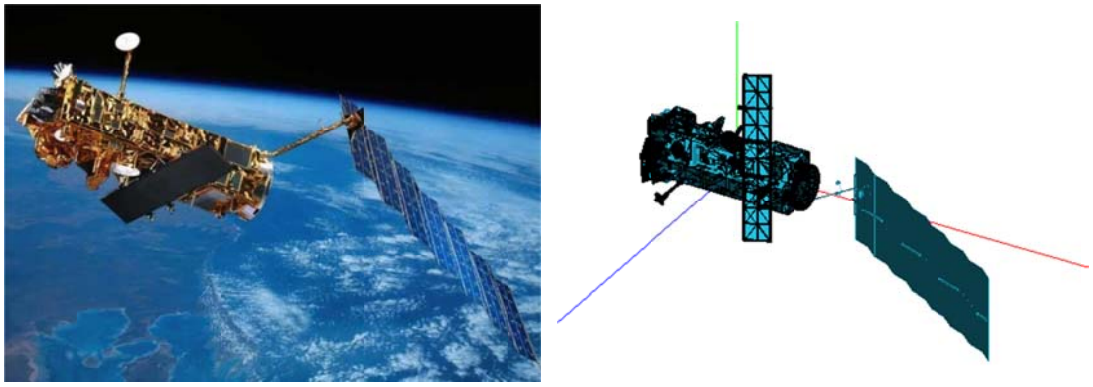

Figure 4-4: ENVISAT satellite in real colors (left panel) and 3D model used in ıOTA tool to generate synthetic SLR and photometric measurements (right panel). Photo credit: ESA and HTG/ıOTA.

4.2.2 ERS-1 and ERS-2

We selected the decommissioned ESA spacecraft ERS-1 (1991-050A) and ERS-2 (1995-021A) as other two priority targets. The ERS-1 mission ended in 2000 after 9 years of service due to a failure of the onboard attitude control system. The satellite is currently in a LEO orbit with a mean altitude around 770 km. ERS-2 was decommissioned in 2011 and its orbit has been lowered from 750 km to 573 km to decrease its lifetime. Both ERS satellites are equipped with RRA and have a very similar design. The 3D model of ENVISAT satellite used in the ıOTA tool is plotted in Figure 4-5.

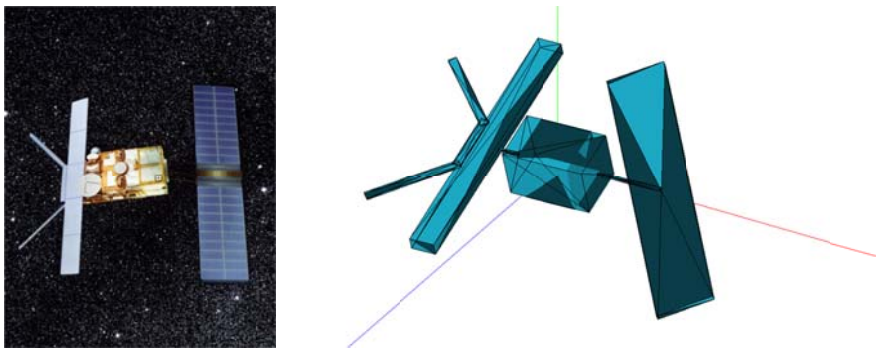

Figure 4-5: ERS-2 satellite in real colors (left panel) and 3D model used in ıOTA tool to generate synthetic SLR and photometric measurements (right panel). Photo credit: ESA and AIUB/HTG/ıOTA.

4.2.3 ADEOS-2

The fourth selected target was ADEOS-2 (2002-056A), a Japan Aerospace Exploration Agency (JAXA) satellite. ADEOS-2 was launched in 2002 into a LEO orbit with a mean orbital altitude around 800 km. After one year of service the mission ended by a failure of the solar panel. Since then the satellite showed several sudden accelera-

tions in rotations. The most current one was observed by ZIMLAT in December 2015. The 3D model of ENVISAT satellite used in the ıOTA tool is plotted in Figure 4-6.

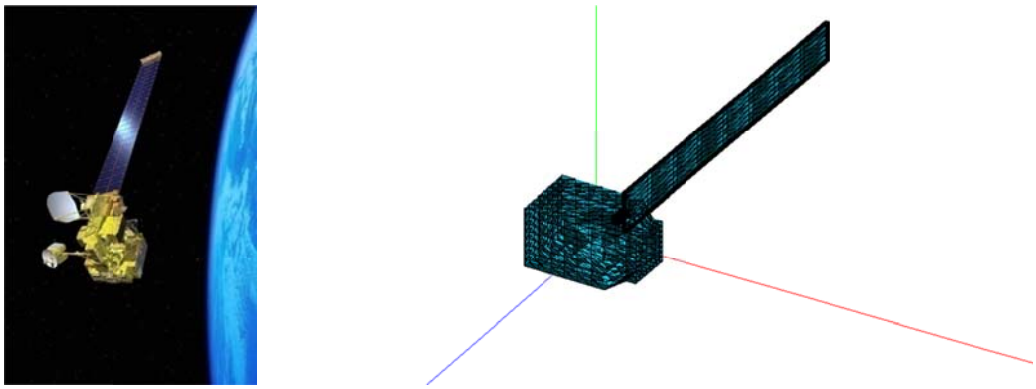

Figure 4-6: ADEOS-2 satellite in real colors (left panel) and 3D model used in ıOTA tool to generate synthetic SLR and photometric measurements (right panel). Photo credit: JAXA and AIUB/HTG/ıOTA.

4.3 Collaborative measurements

The goal of the collaborative observations was to observe the same target at the same time with different types of sensors. These measurements should allow cross-calibration of the different methods and provide testing data for the evaluation of the ıOTA tool.

4.3.1 Selection of observation nights

We had three sensors available for the observation campaign, TIRA, the ZIMLAT telescope and the Graz SLR station. From our five priority targets we selected only objects in LEO. The H-2A R/B could not be observed by any other system than by ZIMLAT (light curve acquisition) due to its high altitude and absence of a RRA.

We investigated the visibilities of ENVISAT, ERS-1, ERS-2 and ADEOS-2 for a time period between Spring and Winter 2016 for all three observation sites. For light curve we required that during the observation the object is illuminated by the Sun while the Sun is below horizon in order to decrease the background noise. We used the following criteria for selecting the correct pass for the simultaneous measurements:

- All objects are illuminated by the Sun
- All objects are above horizon for all stations, preferably > +30° for the Zimmerwald station
- The Sun is below horizon for the Zimmerwald station, preferably below -5°
- Objects are visible from all three sites for at least 3 minutes
- At least one pass of ENVISAT during the given night fulfills the previously listed criteria

Additionally, we included also the following two criteria:

- TIRA is available
- Latest 24 hours before the observation campaign the weather predictions were favorable at least for the Zimmerwald observatory or the Graz SLR station

By following the mentioned criteria we got one month of overlap when we could observe all four targets within one night from all three observation sites. Finally, we selected five nights for collaborative measurements, namely 2016-08-26, 2016-09-04, 2016-09-06, 2016-09-10 and 2016-09-21.

4.3.2 Performed observation campaigns

Due to the weather conditions, we eventually performed collaborative measurements during nights 2016-09-06 and 2016-09-21 only. Unfortunately, the weather conditions at Graz SLR station prevented the station to perform observations during any of the mentioned nights. Therefore, we had simultaneous data from TIRA (ISAR imaging) and ZIMLAT (simultaneous light curve and SLR data). The light curve acquisition at ZIMLAT was performed either by using a CCD camera with frame rates of about 0.75 frames/s or by a sCMOS camera with a frame rates of ~ 5.0 frames/s. The summary of the observations for the nights 2016-09-06 and 2016-09-21 is given in Tab. 1 and 2, respectively.

4.3.3 Night 2016-09-06

The summary of night 2016-09-06 is listed in Table 4-1.

Pass	AIUB SLR	Remark	AIUB LC	Remark	FHR	Remark
ENVISAT 2016-09-06 18:10 UTC	**N/A**	-	**N/A**	-	**YES**	L-band + Ku-band
ENVISAT 2016-09-06 19:47 UTC	**YES**	~400 Interrupted signal	**YES**	CMOS ~400s	**YES**	L-band + Ku-band
ERS-1 2016-09-07 01:43 UTC	**NO**	-	**YES**	CMOS ~250s	**YES**	L-band + Ku-band
ERS-2 2016-09-07 01:51 UTC	**NO**	-	**YES**	CMOS ~120s	**-**	-
Adeos-2 2016-09-07 03:09 UTC	**NO**	-	**YES**	CMOS ~450s	**YES**	L-band + Ku-band
ERS-2 2016-09-07 03:23 UTC	**N/A**	-	**YES**	CCD ~130s	**YES**	L-band + Ku-band

YES – acquisition was successful, data are available, NO – Applicable only for SLR. Attempt to acquire data but un-successful, (N/A) – No attempt.

Table 4-1: Summary of simultaneous observations performed during night 2016-09-06. LC stands for light curve.

As can be seen in Table 4-1, in total there have been six passes (an opportunity to observe) of high priority targets with TIRA and ZIMLAT during the night 2016-09-06, two for ENVISAT, two for ERS-2, one for ERS-1 and one for ADEOS-2. ISAR images with TIRA have been obtained for all six passes and the light curves with ZIMLAT have been obtained for almost all passes except the first ENVISAT pass at 18:10 UTC. For SLR measurements, we were successful only for second ENVISAT pass at 19:57 UTC. Examples of ISAR images obtained by TIRA are plotted in Figure 4-7 and Figure 4-8. For light curves and SLR residuals refer to [AD-7].

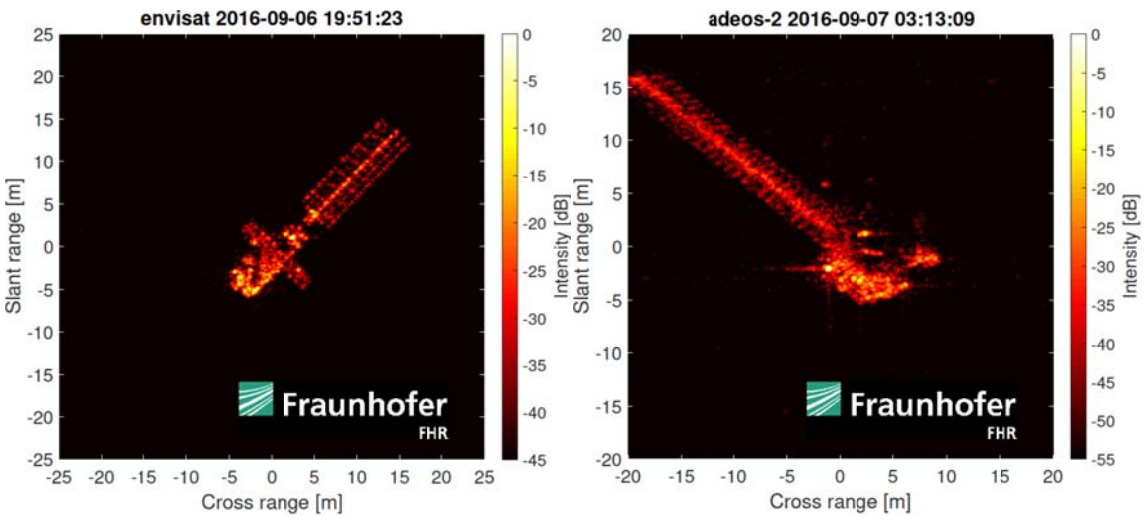

Figure 4-7: ISAR images of ENVISAT (left panel) and ADEOS-2 (right panel) obtained with TIRA during the night 2016-09-06.

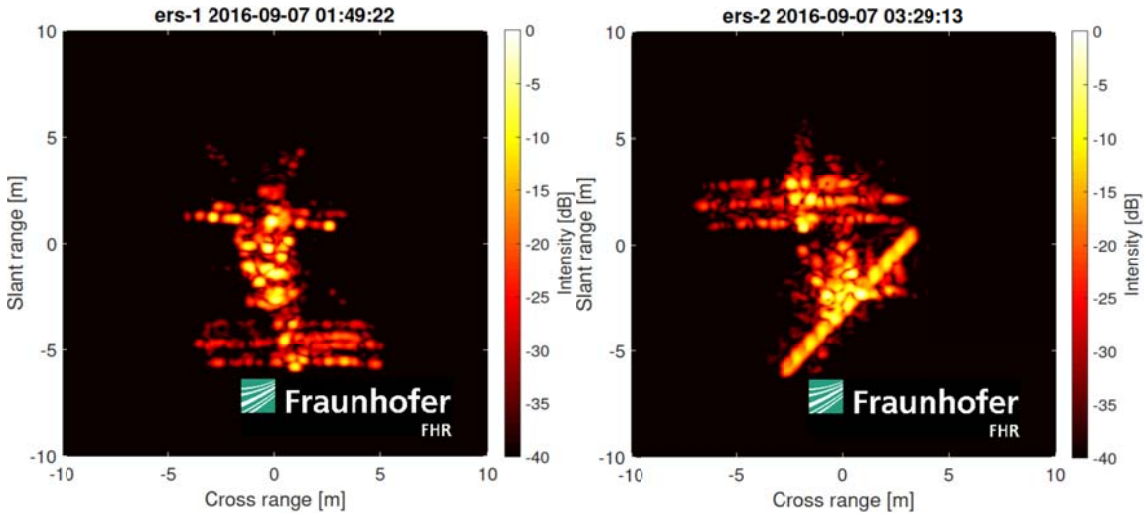

Figure 4-8: ISAR images of ERS-1 (left panel) and ERS-2 (right panel) obtained with TIRA during the night 2016-09-06.

4.3.4 Night 2016-09-21

The summary of night 2016-09-06 is listed in Table 4-2.

Pass	AIUB SLR	Remark	AIUB LC	Remark	FHR	Remark
ENVISAT 2016-09-21 18:57 UTC	**NO**	-	**YES**	CMOS ~300s	**YES**	L-band + Ku-band
ENVISAT 2016-09-21 20:37 UTC	**YES**	~500s Full signal	**YES**	CMOS ~120s	**YES**	L-band + Ku-band
ERS-1 2016-09-22 00:57 UTC	**N/A**	-	**N/A**	-	**YES**	L-band + Ku-band
ERS-2 2016-09-22 02:13 UTC	**NO**	-	**YES**	CMOS ~50s	**YES**	L-band + Ku-band
ERS-1 2016-09-22 02:39 UTC	**NO**	-	**YES**	CMOS ~100s Interrupted	**YES**	L-band + Ku-band
Adeos-2 2016-09-22 03:25 UTC	**NO**	-	**YES**	CMOS ~450s	**YES**	L-band + Ku-band

YES – acquisition was successful, data are available, NO – Applicable only for SLR. Attempt to acquire data but un-successful, (N/A) – No attempt.

Table 4-2: Summary of simultaneous observations performed during night 2016-09-21. LC stands for light curve.

As can be seen in Table 4-2, in total there have been six passes (an opportunity to observe) of high priority targets with TIRA and ZIMLAT during the night 2016-09-21, two for ENVISAT, two for ERS-1, one for ERS-2 and one for ADEOS-2. ISAR images with TIRA have been obtained for all six passes and the light curves with ZIMLAT have been obtained for almost all passes except the first ERS-1 pass at 00:57 UTC. For SLR measurements, we were successful only for second ENVISAT pass at 20:37 UTC. The simultaneously obtained ENVISAT light curve and the SLR measurements can be seen in Figure 4-9. There is clearly a present a signal in

the SLR and light curve signal. In Figure 4-10 and Figure 4-11 are plotted light curves of ENVISAT, ADEOS-2, ERS-1 and ERS-2.

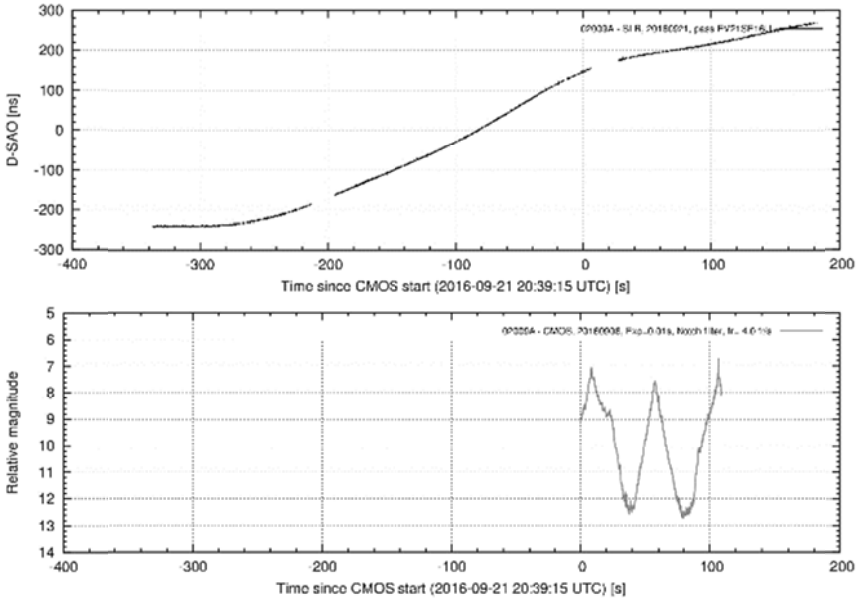

Figure 4-9: SLR residuals of ENVISAT (upper panel) and light curve of ENVISAT (right panel) obtained with ZIMLAT telescope during the second pass at 20:37 UTC during night 2016-09-21.

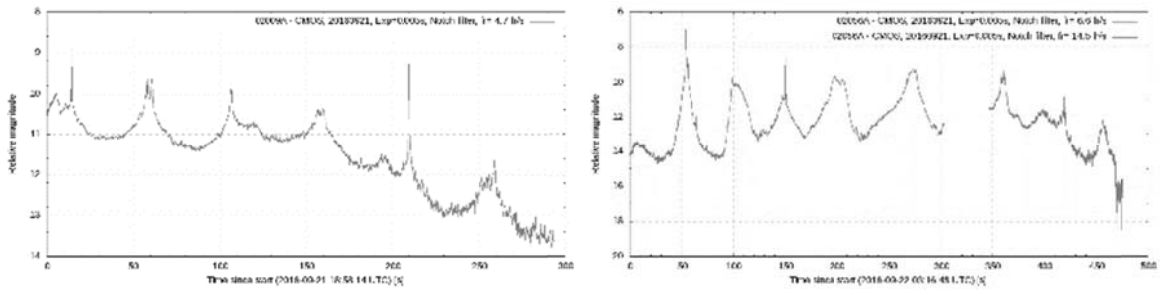

Figure 4-10: ENVISAT (left panel) and ADEOS-2 (right panel) light curves obtained with ZIMLAT telescope during the night 2016-09-21.

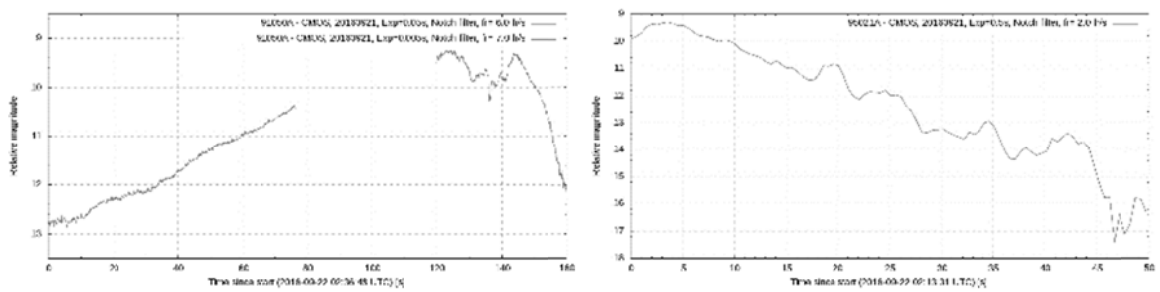

Figure 4-11: ERS-1 (left panel) and ERS-2 (right panel) light curves obtained with ZIMLAT telescope during the night 2016-09-21.

4.3.5 Results from ZIMLAT, light curves

From all obtained light curves, we did extract the apparent rotation period only for ENVISAT. For ADEOS-2 the results were un-conclusive, while for ERS-1 and ERS-2 the rotation was relatively small not allowing to measure the whole rotation of the object around its rotation axis during one pass. We processed three ENVISAT light curves acquired at night 2016-09-06, 19:47 UTC, at 2016-09-21, 18:57 UTC and at 2016-09-21, 20:37 UTC. For the first light curve we extracted apparent period equals to 192.4 s and for the second light curve it was between 195.7 s – 196.9 s. The last light curve has only three peaks covered therefore not the full rotation has been measured. From these three peaks and by using peak-to-peak analysis we estimated apparent rotation period to be 196.9 s. The results are summarized in Table 4-3.

Pass	Apparent rotational velocity [deg/s]	Apparent rotational velocity [deg/s]
ENVISAT 2016-09-0619:47 UTC	192.4	1.8711
ENVISAT 2016-09-2118:57 UTC	195.7 – 196.6	**1**.8400 – 1.8283
ENVISAT 2016-09-2120:37 UTC	196.92	1.8282

Table 4-3: Estimated apparent rotational velocity vectors from light curves.

4.3.6 Results from ZIMLAT, SLR

There were in total two SLR measurements obtained for ENVISAT during collaborative measurement campaign. The first measurements obtained during night 2016-09-06, 19:47 UTC (see **Error! Reference source not found.**, upper panel) had a strongly interrupted signal and could not be further processed. For the second pass 2016-09-21, 20:37 UTC (see Figure 4-9, upper panel) we detrended the SLR signal by improving the along-track component for the satellite position. This pre-processed signal can be seen in Figure 4-12. The obtained signal has been further processed by using AIUB's SLR fitting method discussed section 2.3.3 during which we obtained stable solutions consistent with our previous findings. The obtained coefficients are listed in Table 4-4. Furthermore, we used the ENVISAT Two Line Elements (TLE) from given date and we transformed the obtained coefficients to the Earth-centered inertial coordinate (ECI) True Equinox Mean Equator (TEME) reference frame (ECI/TEME). The calculated vector components are listed in Table 4-4.

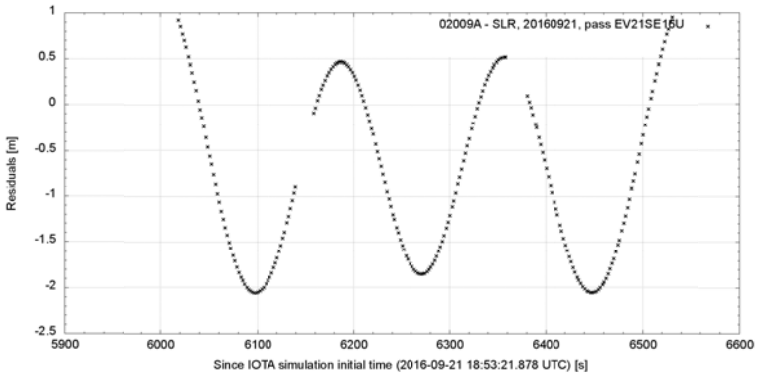

Figure 4-12: Detrended SLR residuals of ENVISAT obtained with ZIMLAT telescope during the second pass at 20:37 UTC during night 2016-09-21 by improving the along-track component for the satellite position.

Coefficient	Value
Ref. epoch (UTC)	2016-09-21 20:33:36.589
Ref. epoch (MJD) [day]	57652.85667349

γ [deg]	168.7271
γ_{phase} [deg]	26.7424
β [deg]	59.7064
$P_{inertial}$ [s]	214.6206
$\omega_{inertial}$ [deg/s]	1.6775

Table 4-4: Coefficients estimated by using AIUB's fitting method for ENVISAT pass 2016-09-21, 20:37 UTC.

Pass	Rotation vector [rad/s]			Apparent rotational velocity [deg/s]
ENVISAT 2016-09-2120:37 UTC	2.115e-2	1.803e-2	9.189e-3	1.6782

Table 4-5: Estimated rotational velocity vector in ECI/TEME coordinates obtained from SLR residuals of ENVISAT pass 2016-09-21, 20:37 UTC.

4.3.7 Results from TIRA

4.3.7.1 Attitude estimation with ıOTA

Attitude estimation using the simulator ıOTA needs much more computational power than assuming a fixed rotational velocity vector in the inertial system (several hours for the optimization with ıOTA vs. less than a minute for the optimization without ıOTA). Therefore, only one passage of ENVISAT was analysed by this method (see [3] for the temporal investigation of ENVISAT's rotational motion using the first optimization procedure). Figure 4-13 shows ISAR images of ENVISAT with overlaid WGMs. For testing purposes, first a CAD model of a sphere and a corresponding inertia tensor proportional to the unit matrix were applied. Doing so, the ıOTA result essentially gave the same mean square error (MSE) as the algorithm designed for a constant rotational velocity vector, and the initial attitude and rotational velocity vector differed only slightly. This confirmed the ıOTA simulation program. Comparing the attitude quaternions generated by ıOTA for subsequent time instances, it could be observed that the rotational velocity vector simulated by ıOTA kept nearly constant as expected for a spherical object.

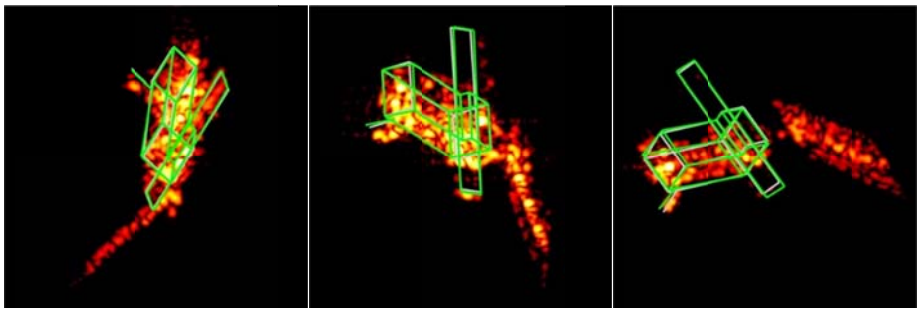

Figure 4-13: ISAR images of ENVISAT with superposed WGMs (green: manual projection, grey:automatic projection) after the optimization procedure.

In a next step, the sphere was replaced by an ENVISAT CAD model along with the corresponding inertia tensor. Several error minimization procedures were tested. First, the estimate for constant rotation vector was taken for initialization. Then, random initialization was tried, leading in one case to an error reduction. The alternative error measure was also used in other cases as shown in Table 4-6. Using this measure led to similar results as the original one. Surprisingly, the original error measure was reduced by using the alternative error measure for minimization. The error measure could be further reduced by taking the result as initialization of subsequent error minimization with the original error measure. The resulting root mean square (RMS) position errors are given in Table 4-6.

All results refer to a minimization where WGM projections due to WGM matching to single images were taken as reference points in the image. Unexpectedly, for all procedures using ιOTA the RMS error was higher than the RMS error for the constant rotational velocity assumption. The reason for this is not yet clear. A possible cause could be that the CAD model and/or its center of gravity and inertia tensor do not sufficiently match reality. Alternatively, the algorithm may not converge to the absolute minimum of the error function but to a relative minimum.

Physical model for optimization	Initialization	RMS position error [m]
constant rotation vector	random	0.14603
ιOTA with error from all projected WGM points	initialized by constant rotation vector result	0.99460
ιOTA with error from all projected WGM points	random, 4 trials	3.69647 3.10312 3.10106 3.16018
ιOTA with alternative error measure	constant rotation vector result	4.77809
ιOTA	Result from previous case	2.06387

Table 4-6: RMS error of point positions for different simulation and computation procedures (ENVISAT 2016-09-06 19:48 UTC).

4.3.7.2 Attitude estimation without ιOTA

Table 4-7 gives the estimated velocity vectors for the different radar observations under the assumption of a constant rotation vector. ISAR images of the different objects are shown in Figure 4-8.

While the WGM for ENVISAT was derived from a CAD model, the WGMs for the other satellites were derived by hand from data sheets provided by ESA. Therefore, these WGMs might be inaccurate.

The assumption of constant rotation vector appears to be satisfied for all ENVISAT and ERS-1 passes. For ERS-2, this assumption seems to be satisfied only for the pass on 22 Sept. 2016. The pass on 07 Sept. 2016 was divided in 3 sub-passes. Individual rotation velocity vectors were fitted under the assumption of constant rotation vector over each sub-pass.

ADEOS-2 is a strongly tumbling object and the assumption of constant rotation velocity vector is not fulfilled. Therefore, it was not possible to derive a rotation vector from both passages.

Pass	Rotation vector [rad/s]			Rotational velocity [deg/s]
ENVISAT 2016-09-0618:11 UTC	2.55e-02	1.16e-02	-1.60e-03	1.6066
ENVISAT 2016-09-0619:48 UTC	2.64e-02	1.16e-02	3.85e-03	1.6683
ERS-1 2016-09-0701:43 UTC	8.92e-03	4.48e-03	-5.53e-03	0.6540
ERS-2 2016-09-0703:24 UTC	3.51e-03 8.57e-03 4.71e-03	-2.79e-03 -5.16e-04 -1.65e-03	-6.96e-03 1.41e-02 5.57e-03	0.4743 0.9896 0.4282
ADEOS-2 2016-09-0703:09 UTC	-			-
ENVISAT 2016-09-2118:53 UTC	1.94e-02	2.12e-02	8.69e-04	1.6498
ENVISAT 2016-09-2120:32 UTC	1.52e-02	2.43e-02	1.93e-03	1.6442
ERS-1 2016-09-2200:54 UTC	-1.29e-02	3.62e-03	1.45e-03	0.7700
ERS-2 2016-09-2202:10 UTC	1.30e-02	-1.38e-04	-8.25e-03	0.8829
ERS-1 2016-09-2202:34 UTC	1.99e-03	-5.99e-04	5.09e-03	0.3149
ADEOS-2 2016-09-2203:25 UTC	-			-

Table 4-7: Estimated rotational velocity vectors in ECI coordinates (01.January 2000 12:00 UT).

4.3.8 Results comparison, methods cross-check

Three independent solutions have been found for the ENVISAT rotation axis direction in ECI for the passes from night 2017-09-21. Two solutions have been obtained from the ISAR images, one from pass 18:53 UTC and from pass 20:32 UTC (see Table 4-7), and one solution from the SLR residuals from pass 20:32 UTC (see Table 4-5). To these solutions we will refer as to the solution no. 1, no. 2 and no. 3, respectively. Each of the solutions (unit vectors) have been transformed to the tOTA input formats, namely to the inertial Roll, Pitch and Yaw angles and rotation vectors $\boldsymbol{\omega}$. Solutions no. 1.0 and 3.0 have been further refined to achieve a match between the synthetic and real measured SLR residuals. The refined solution from ISAR and pass 18:53 UTC (solution no. 1.1) has been found by integrating the attitude motion (solution no. 1.0) to the second pass at 20:37 UTC for which the SLR residuals are available. The input parameters have been improved to match the synthetic SLR residuals with the real SLR residuals, namely their peaks were aligned. All the relevant acting forces have been included during integration. The SLR time corrected solution (no. 3.1) has been found by using the original SLR solution (no. 3.0) and by correcting the initial reference time to get the match between the synthetic SLR residuals and real SLR residuals. The reference time was changed from 20:33:36.6 to 20:31:18.6 UTC. All the solutions, the rotation vectors in the ECI coordinates, are listed in Table 4-8. For solutions no 3.0 and no. 3.1 the vectors are identical. This is because the solution no. 3.1 was found by refining the reference time not the vector itself.

Pass	Rotation vector [rad/s]			Apparent rotational velocity [deg/s]
ISAR (solution no 1.0) ENVISAT 2016-09-2120:37 UTC	0.0194	0.0212	0.0009	1.6498
ISAR (solution no 1.1) ENVISAT 2016-09-2120:37 UTC	0.0200	0.0199	0.0066	1.6597
ISAR (solution no 2.0) ENVISAT 2016-09-2120:37 UTC	0.0152	0.0243	0.0019	1.6442
SLR (solution no. 3.0) ENVISAT 2016-09-2120:37 UTC	0.0212	0.0180	0.0092	1.6782
SLR, refined (solution no. 3.1) ENVISAT 2016-09-2120:31 UTC	0.0212	0.0180	0.0092	1.6782

Table 4-8: Estimated rotational velocity vectors for solutions. Solutions from ISAR are in ECI/J2000 coordinates (01.January 2000 12:00 UT) and from SLR in ECI/TEME coordinates.

All five obtained solutions agreed on the attitude motion of ENVISAT, that the rotation of the satellite during the observations was mostly around the z-axis as shown in Figure 4-14. All solutions also agree on the size of the rotation vector which was found to be between -1.64 deg/s and -1.68 deg/s (see Table 4-5 and Table 4-7).

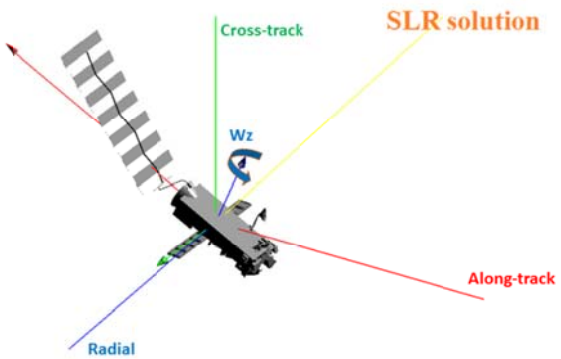

Figure 4-14: Graphical representation of the ENVISAT rotation as determined from the ISAR images and SLR residuals. Both solutions agree on the vector-body alignment and on the rotation vector size.

For demonstration purposes, we will show the results obtained for the solution no. 1.1 only. For more information about other solutions refer to [AD-5]. For simulation no 1.1 covered have been both passes, 18:53 UTC and 20:32 UTC. Obtained synthetic measurements have been compared to the real measurements, SLR (acquired by ZIMLAT) and ISAR images (acquired by TIRA). This comparison also suited as a methods cross-check.

4.3.8.1 Pass “18:53 UTC”

For this pass the simulated data showed no SLR residuals as was the case during the real SLR measurements. There was a very good match between the simulated ISAR images (see Figure 4-15, middle panels) and the real ones (see Figure 4-15, right panels). For completeness, also the simulated direct images are displayed in Figure 4-15, left panels. The simulated data in Figure 4-15 are for the same reference time as the real data (upper part of the right panels).

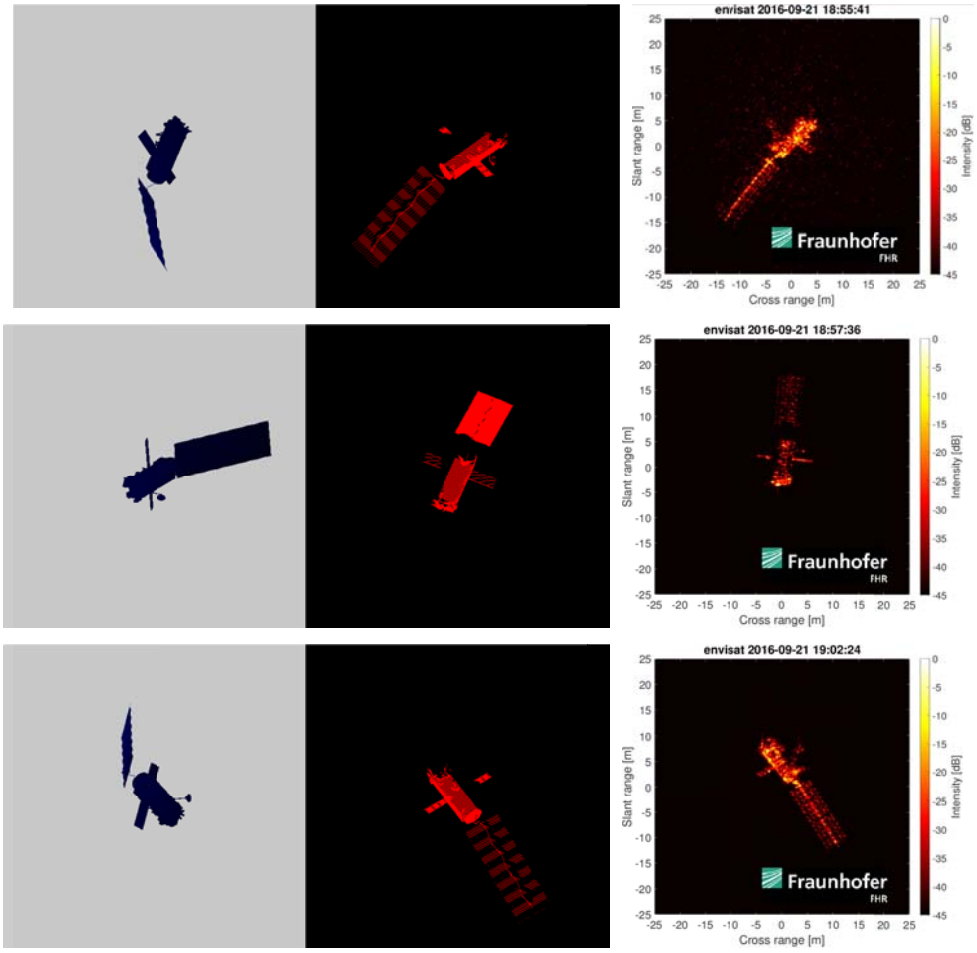

Figure 4-15: Real ISAR image (right panel) acquired by TIRA versus synthetic ISAR image (middle panel) and synthetic direct image (left panel) generated by IOTA for solution with ID 1.1 ("refined ISAR solution 18:53 UTC").

4.3.8.2 Pass "20:32 UTC"

For this pass the simulated data showed a full SLR residuals signal as shown in Figure 4-16 (blue points) as it was also observed during the real measurements (red points). The match between the simulated and real SLR residuals is very good. The peaks match quite good on the horizontal time axis, as well on the vertical range axis. Same goes for ISAR images. In Figure 4-17 are plotted real ISAR images (right panels) against simulated ISAR images (middle panels).

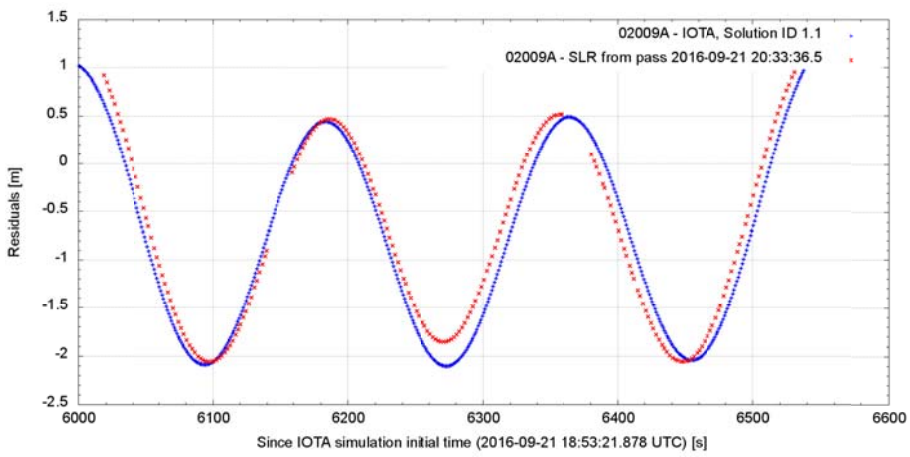

Figure 4-16: Real SLR residuals (red points) acquired by ZIMLAT telescope versus synthetic SLR residuals generated by IOTA (red points) for solution with ID 1.1 ("refined ISAR solution 18:53 UTC").

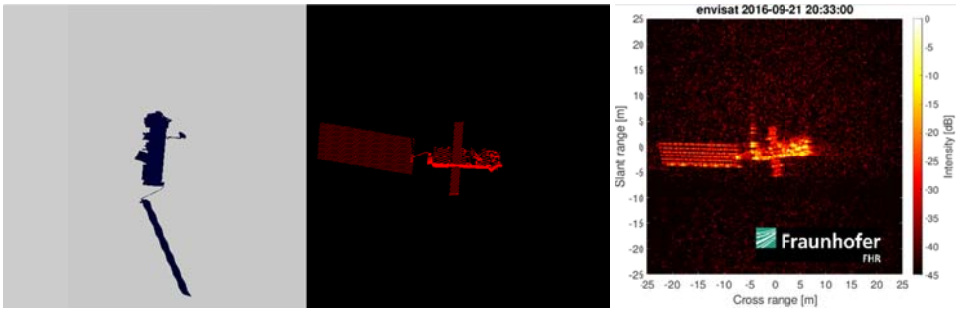

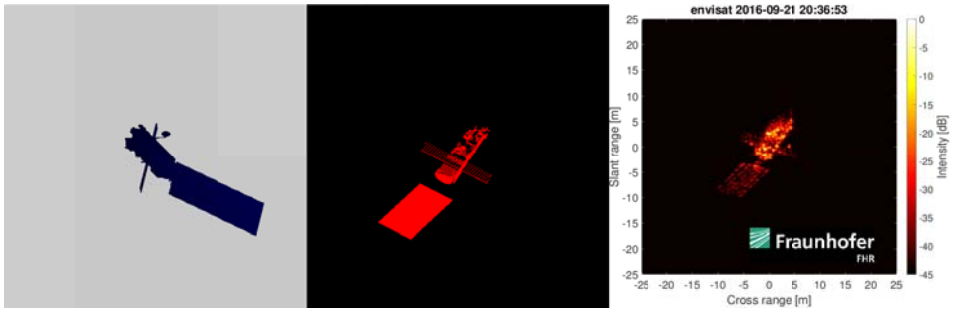

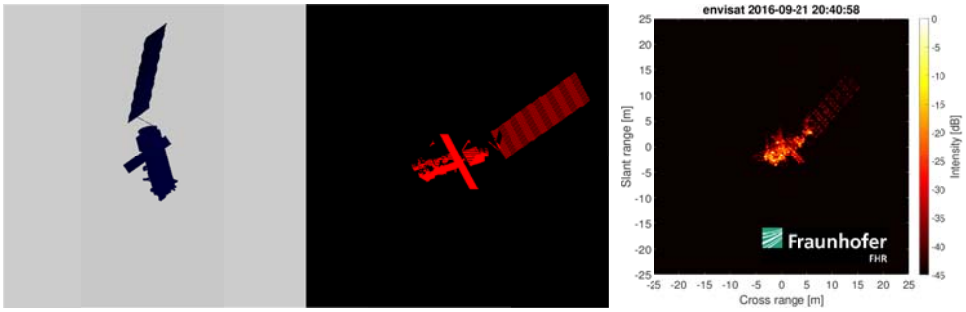

Figure 4-17: Real ISAR image (right panel) acquired by TIRA versus synthetic ISAR image (middle panel) and synthetic direct image (left panel) generated by IOTA for solution with ID 1.1 ("refined ISAR solution 18:53 UTC").

5 CONCLUSIONS AND SUMMARY

The presented activity was dedicated to the attitude determination of space debris objects such as defunct spacecraft and upper stages by using different types of observation techniques. The main objective was to provide this type of information during contingency cases and for future Active Debris Removal (ADR) missions. In our work, we focused on the observation techniques which are related to the attitude determination, namely the Inverse Synthetic Radar Images (ISAR), Satellite Laser Ranging (SLR) and light curves. All these techniques and with them related processing have been reviewed and improved during our activity where Fraunhofer Institute for High Frequency Physics and Radar Techniques (FHR) was responsible for the ISAR, the Astronomic Institute of the University of Bern (AIUB) for light curves and the Space Research Institute's (IWF) for SLR.

A development of a highly modular software tool ıOTA has been performed by the Hypersonic Technology Goettingen (HTG). This tool performs short- (days) to long-term (years) propagations of the orbit and of the attitude motion of a spacecraft taking into an account all the relevant acting forces and torques. Furthermore, ıOTA's postprocessing modules generate synthetic measurements, e.g. light curves, SLR residuals and ISAR images that can be compared with the real measurements. The strength of the approach is the combination of various attitude measurement types to cancel ambiguities of the individual methods and to combine this information with a dynamic model to establish attitude prediction. The validation of the attitude model has been done by comparison to real observations of targets with known attitude states.

Four targets have been selected for a collaborative observation campaign. These targets have been defunct LEO satellites ENVISAT, ERS-1, ERS-1 and ADEOS-2. Collaborative observations have been performed during two nights in September 2016, 6th and 21st. The ISAR images and light curves have been acquired for all targets by FHR's TIRA and AIUB's ZIMLAT system, respectively. The SLR residuals have been acquired by AIUB's ZIMLAT system and have been obtained only for ENVISAT. The attitude could be determined for ERS-1 and ERS-2 by using ISAR images. For ADEOS-2 the solution was non-conclusive which indicates highly tumbling stage for this target. For ENVISAT the attitude state has been found by using ISAR and SLR measurements.

There were in total two passages of ENVISAT over Europe during the night 2016-09-21 when the satellite was visible for the optical passive sensors. Two light curves and one set of SLR residuals have been acquired by using AIUB's ZIMLAT system. At the same time, ENVISAT was observed by the FHR's TIRA from which the ISAR images were obtained. The ISAR images provided solution for the rotation vector direction and its size in ECI reference frame. The SLR residuals provided this vector for the second passage only. All three solutions agree that the rotation of the satellite during the observations was mostly around the z-axis. The both solutions also agreed on the size of the rotation vector which was found to be between -1.64 deg/s and -1.68 deg/s.

Furthermore, the obtained solutions for ENVISAT rotation vector have been used to generate synthetic measurements with ıOTA. These were then used to refine by getting the best match between the real and synthetic SLR measurements. With this approach, we found the ENVISAT rotation vector for which the real and synthetic ISAR and SLR measurements are in very good match. This result was presented in this report. This test also served as an independent method cross-check for validating the ISAR, SLR and ıOTA attitude determination techniques.